

## Article

# Effects of Low Temperatures on Flexural Strength of Macro-Synthetic Fiber Reinforced Concrete: Experimental and Numerical Investigation

Stanislav Aidarov <sup>1,\*</sup>, Alejandro Nogales <sup>1</sup>, Igor Reynvart <sup>1</sup>, Nikola Tošić <sup>2</sup> and Albert de la Fuente <sup>2</sup>

<sup>1</sup> Smart Engineering Ltd., UPC Spin-Off, Jordi Girona 1-3, 08034 Barcelona, Spain; alejandro.nogales@upc.edu (A.N.); igor.reynvart@estudiant.upc.edu (I.R.)

<sup>2</sup> Civil and Environmental Engineering Department, Universitat Politècnica de Catalunya (UPC), Jordi Girona 1-3, 08034 Barcelona, Spain; nikola.tosic@upc.edu (N.T.); albert.de.la.fuente@upc.edu (A.d.l.F.)

\* Correspondence: stanislav.aidarov@upc.edu

**Abstract:** Fiber-reinforced concrete (FRC) is an attractive alternative to traditional steel bar-reinforced concrete structures, as evidenced by the constantly increasing market consumption of structural fibers for this purpose. In spite of significant research dedicated to FRC, less attention has been given to the effects of low temperatures on the mechanical properties of FRC, which can be critical for a variety of structural typologies and regions. With this in mind, an experimental program was carried out to assess the flexural behavior of macro-synthetic fiber-reinforced concrete (MSFRC) at different temperatures (from 20 °C to −30 °C) by means of three-point bending notched beam tests. The tested MSFRCs were produced by varying the content of polypropylene fibers (4 and 8 kg/m<sup>3</sup>). The results proved that the flexural strength capacity of all MSFRCs improved with decreasing temperature. Finite element analyses were then used to calibrate constitutive models following *fib* Model Code 2010 guidelines and to formulate empirical adjustments for taking into account the effects of low temperatures. The outcomes of this research are the basis for future experimental and numerical efforts meant to improve the design of MSFRCs subjected to low temperatures during service conditions.

**Keywords:** polymeric fiber reinforced concrete; experimental program; temperature variation; residual tensile strength; one-way element; beam; non-linear analysis; modeling

**Citation:** Aidarov, S.; Nogales, A.; Reynvart, I.; Tošić, N.; de la Fuente, A. Effects of Low Temperatures on Flexural Strength of Macro-Synthetic Fiber Reinforced Concrete: Experimental and Numerical Investigation. *Materials* **2022**, *15*, 1153. <https://doi.org/10.3390/ma15031153>

Academic Editor: Karim Benzarti

Received: 25 December 2021

Accepted: 30 January 2022

Published: 2 February 2022

**Publisher's Note:** MDPI stays neutral with regard to jurisdictional claims in published maps and institutional affiliations.



**Copyright:** © 2022 by the authors. Licensee MDPI, Basel, Switzerland. This article is an open access article distributed under the terms and conditions of the Creative Commons Attribution (CC BY) license (<https://creativecommons.org/licenses/by/4.0/>).

## 1. Introduction

Fiber-reinforced concrete (FRC) is one of several new types of innovative concretes that can be used for structural purposes in accordance with a number of national and international codes, guidelines, and design recommendations [1–6]. The incorporation of fibers in cement-based composites allows the partial or even total substitution of traditional reinforcement (reinforcing steel bars) with a positive effect on the fracture energy of the matrix [7], cracking control [8–12], fire resistance [13–15], fatigue [16,17], redistribution capacity [18–21], and impact resistance [22–25]. As a result, the application of FRC is already observed in a multitude of structural elements, such as precast tunnel segments [26–28], elevated flat slabs [29–31], reinforced earth-retaining walls [32], and ground-supported flat slabs for industrial applications [33,34].

Moreover, numerous research programs are focused on the material characterization of FRC [35–39] and the further elaboration of both analytical [40–46] and numerical [47–51] design approaches to suitably evaluate the response of FRC elements under diverse load/boundary conditions. However, the majority of research studies tend to evaluate the mechanical performance of FRC subjected to normal temperature conditions or high/extremely high (e.g., fire) temperatures. In contrast, the behavior of FRC at low temperatures

is scarcely analyzed, although there are a number of possible scenarios in which it would be essential to adequately predict its structural response under relatively adverse conditions, e.g., (1) the storage (Figure 1), handling, and transportation of precast tunnel segments in cold regions or (2) the service life of industrial floors for cold-storage warehouses.



**Figure 1.** Precast concrete elements subjected to low temperatures (reproduced with permission from [52]).

Drawing an analogy with plain or traditionally reinforced concrete under these conditions, an increase in compressive and tensile strength can be expected [53,54] along with the embrittlement of a concrete matrix [55]. Taking into account the increased tensile strength of the material, sufficient ductility to the structural element must be provided by the reinforcement once cracking occurs. In the case of FRC, residual tensile strength is mainly responsible for the post-cracking behavior of the material—this property should also be improved as the matrix–fiber interaction enhances with decreasing temperatures as long as the mechanical properties of the fibers are not negatively affected by external conditions.

However, to the authors' best knowledge, only a few experimental investigations were dedicated to examining the influence of low temperatures on the post-cracking response of FRC with moderate values of compressive strength (up to 60 MPa). Pigeon and Cantin [56] highlighted the slight and significant increase in steel fiber reinforced concrete (SFRC) toughness at  $-10\text{ °C}$  and  $-30\text{ °C}$ , respectively. Caballero-Jorna et al. [57] emphasized a minor enhancement of the post-cracking flexural strength of SFRC and MSFRC at  $-15\text{ °C}$ , whereas Richardson and Ovington [58], on the contrary, stressed a considerably greater flexural strength of both SFRC and MSFRC at  $-20\text{ °C}$ . Despite the obtained results, there is still a lack of information for modeling possible “temperature–post-cracking flexural strength” relationships for different types of FRC and, more importantly, the adjusted designed procedures to suitably predict the structural response of FRC at low temperatures have still not been analyzed.

With this in mind, the presented research study was conducted, this being comprised of two main parts. Primarily, an experimental program was carried out in order to characterize pre- and post-cracking flexural behavior of FRC at different temperatures (from  $20\text{ °C}$  to  $-30\text{ °C}$ ): the standardized three-point bending test (3PBT) on a notched beam ( $150 \times 150 \times 600\text{ mm}^3$ ) according to EN 14651 [59]. For the sake of more detailed analysis, two types of FRC were characterized: MSFRC with fiber contents of  $4\text{ kg/m}^3$  (MSFRC-4) and  $8\text{ kg/m}^3$  (MSFRC-8).

Thereafter, multi-linear constitutive models were derived pursuant to the *fib* Model Code 2010 [1] in order to simulate experimentally obtained “load–displacement” curves at  $20\text{ °C}$ ,  $0\text{ °C}$ ,  $-10\text{ °C}$ , and  $-30\text{ °C}$ . Moreover, correction factors to the elaborated constitutive diagrams were identified with the aim of fitting the numerical prediction to the real behavior of the tested beams.

As a result, the experimental outcome enlarged existing databases on FRC mechanical performance and allows practitioners to consider the mechanical properties of FRC when designing for cold climates or conditions where low temperatures are expected. Additionally, the numerical part of the study evidenced the necessity of the correction factors to precisely predict the real behavior of FRC elements reinforced by a given amount/type of fibers.

## 2. Experimental Program

### 2.1. Concrete Mix


The adopted mix (Table 1) corresponded to the normal strength concrete and S3 consistency class, i.e., the measured slump was between 100 and 150 mm [60]. A Portland cement type CEM II-A/L was used for producing the MSFRC mixes. The concrete matrix consisted of three aggregate sizes: sand 0/4, gravel 4/10, and gravel 10/20 from crushed calcareous stone. A lignosulphonate-based plasticizer and a polycarboxylate-based superplasticizer were also added during the material elaboration in order to provide the required workability of the mix.

**Table 1.** Composition of studied MSFRC.

Materials	MSFRC-4	MSFRC-8
CEM II-A/L 42.5R (kg/m <sup>3</sup> )	310	310
Coarse aggregate 10/20 (kg/m <sup>3</sup> )	690	680
Coarse aggregate 4/10 (kg/m <sup>3</sup> )	127	125
Fine aggregate 0/4 (kg/m <sup>3</sup> )	1025	1025
Water-cement ratio	0.58	0.58
Additives (% on cement content)	1.2	1.5
Synthetic fibers (kg/m <sup>3</sup> )	4	8

Based on the described concrete composition, two types of FRC were produced: polypropylene fiber-reinforced concrete with a fiber content of (1) 4 kg/m<sup>3</sup> (volume fraction 0.425%) and (2) 8 kg/m<sup>3</sup> (volume fraction 0.850%); Table 2 gathers the essential properties of the used polypropylene fiber (PPF). MSFRC-4 was oriented to industrial floors in which only the minimum reinforcement is required to control cracking due to thermal–hydro-metric (temperature and shrinkage gradients) phenomena. In turn, MSFRC-8 was selected to reproduce medium-heavy duty pavements, which, apart from the previously mentioned indirect loads, could be subjected to external loads of notable magnitude.

**Table 2.** Properties of the implemented fiber.

Property	PPF	Representation
Material	Transparent polypropylene	
Shape	Embossed monofilament	
Diameter (mm)	0.85	
Length (mm)	48	
Aspect ratio	56.5	
Number of fibers per kg	41,200	
Tensile strength (MPa)	>400	

### 2.2. Test Setup and Testing Procedure

The structural response of the elaborated MSFRC mixes in terms of flexural pre- and post-cracking strengths was analyzed at 20 °C (reference temperature), 0 °C, −10 °C, and −30 °C. This mechanical property of the studied MSFRC was assessed in compliance with EN 14651 [59] (Figure 2a) by testing six notched prismatic beams (150 × 150 × 600 mm) for each temperature magnitude, resulting in 48 tested samples. The casting and demolding

(in 24 h) of the prismatic beams in question were followed by the curing of these specimens in a temperature (20 °C) and humidity (95%) controlled chamber for 28 days.

Thereafter, three-quarters of all beams were placed in a laboratory freezer, and each quarter was cooled to 0 °C, −10 °C, and −30 °C, respectively. Importantly, the prismatic samples were equipped with a thermocouple in order to guarantee the target test temperature and, additionally, to monitor its evolution (Figure 2b). Once the required temperature was reached, the specimens were placed in an INSTRON 8505 testing machine (Figure 2c) equipped with a load cell of 100 kN in order to estimate the flexural behavior. The parameters of major concern within the testing procedure were the limits of proportionality ( $f_{LOP}$ ),  $f_{R1}$ , and  $f_{R3}$ ;  $f_{LOP}$  represented the pre-cracking flexural behavior, whereas the residual tensile strengths  $f_{R1}$  and  $f_{R3}$  were used to derive the constitutive models of the MSFRC for design purposes, being related with serviceability and ultimate limit states, respectively.



Figure 2. (a) 3PBT setup; (b) freezing procedure and temperature monitoring; (c) 3PBT at −30 °C.

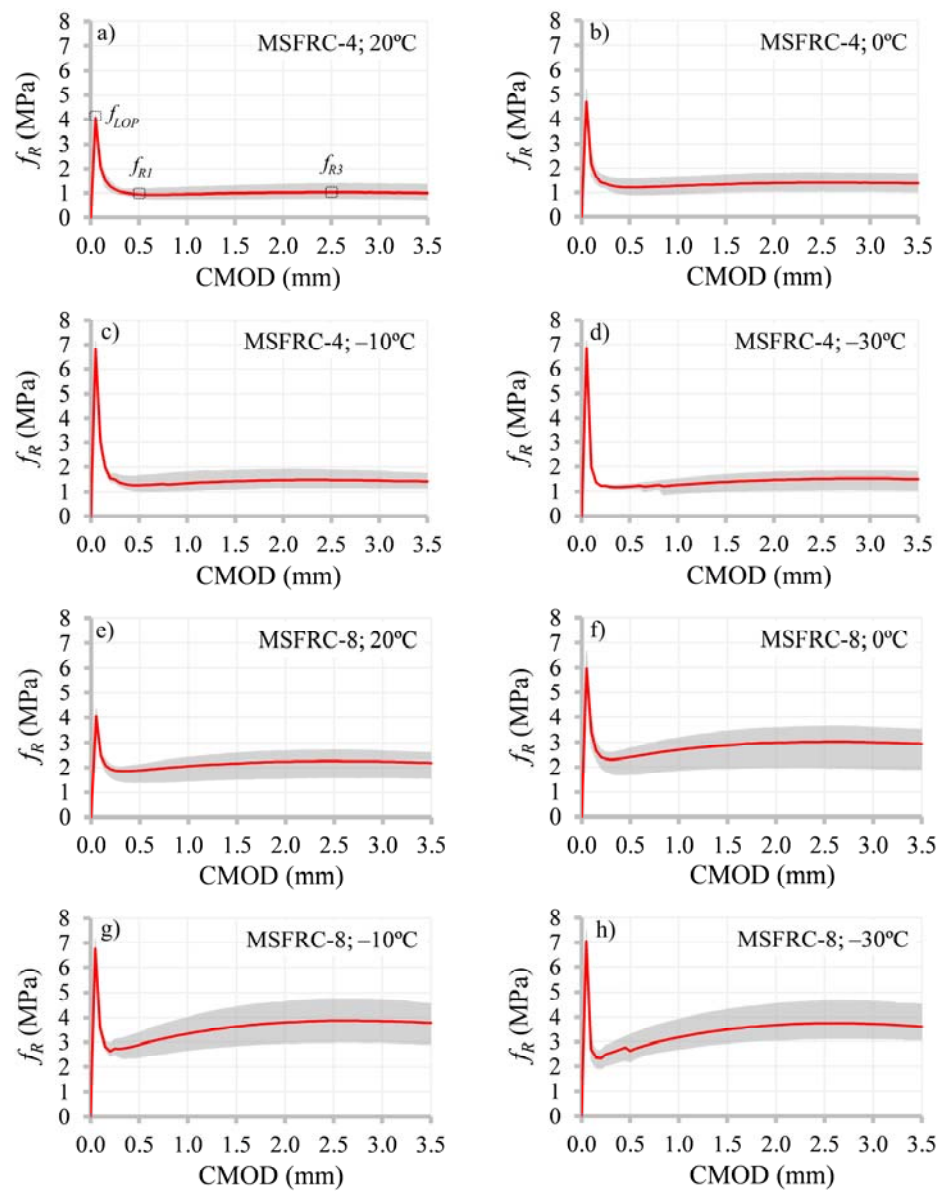
### 3. Experimental Results and Discussions

Figure 3 gathers responses obtained by means of the 3PBT in terms of pre- and post-cracking strength and crack mouth opening displacement (CMOD); average values are highlighted by red lines (based on six tested specimens for each case), whereas result scatter (envelope) is represented by a shaded area. Primarily, pre-cracking behavior was assessed for both MSFRC-4 and MSFRC-8. Taking into consideration that this mechanical property is mainly dependent on the material matrix [61,62] (amount of cement paste and granular skeleton), similar results were expected regardless of the fiber content.

This expectation was proven accurate, as seen in Figure 4—the limit of the proportionality of MSFRC-4 and MSFRC-8 at the reference temperature was almost identical. Decreasing the temperature to the threshold value for water to start freezing (0 °C),  $f_{LOP}$  started increasing by 15.8% and 47.0% for MSFRC-4 and MSFRC-8, respectively. Further reduction in the temperature led to a significant enhancement of  $f_{LOP}$ : a total increment of 67.7% and 66.5% was detected for the above listed materials at −10 °C, whereas the temperature magnitude of −30 °C entailed an increment of 68.5% and 73.2% for MSFRC-4 and MSFRC-8, respectively (comparing with  $f_{LOP}$  at 20 °C).

Thereafter, the effect of the temperature variation on the residual tensile strengths ( $f_{R1}$ ,  $f_{R3}$ ) was estimated. This mechanical parameter, apart from the characteristics of the concrete matrix, depends on a certain number of factors, such as the mechanical properties of the implemented fibers, fiber geometry (having a main effect on anchorage and bond capacity), and fiber distribution and orientation within the critical section. Therefore, the analysis of post-cracking behavior of FRC at low temperatures is a challenging aspect to be investigated.





**Figure 3.** Flexural pre- and post-cracking strength at different temperatures of: (a–d) MSFRC-4; (e,f) MSFRC-8.

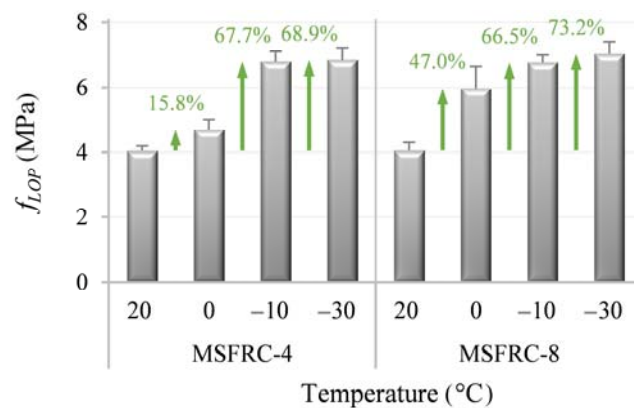


**Figure 4.** Mean values of  $f_{LOP}$  with corresponding standard deviations of the studied MSFRCs at different temperatures.

The results that can serve as a base for further investigations are presented in Figure 5. Analyzing the observed structural response of the tested FRC beams, the positive effect of low temperatures on the energy required to produce fiber pull-out can be emphasized, i.e., the concrete matrix that embeds the fibers shrinks with the decrease in temperature, provoking an increase in confinement pressure along the fibers and thus enhancing the anchorage capacity of fibers. This phenomenon, in turn, improves the post-cracking flexural behavior as it was depicted in [63,64]. Importantly, the studied range of temperatures had no detectable negative influence on the mechanical properties of the implemented fibers and, thereby, on the overall performance of the studied FRC beams.

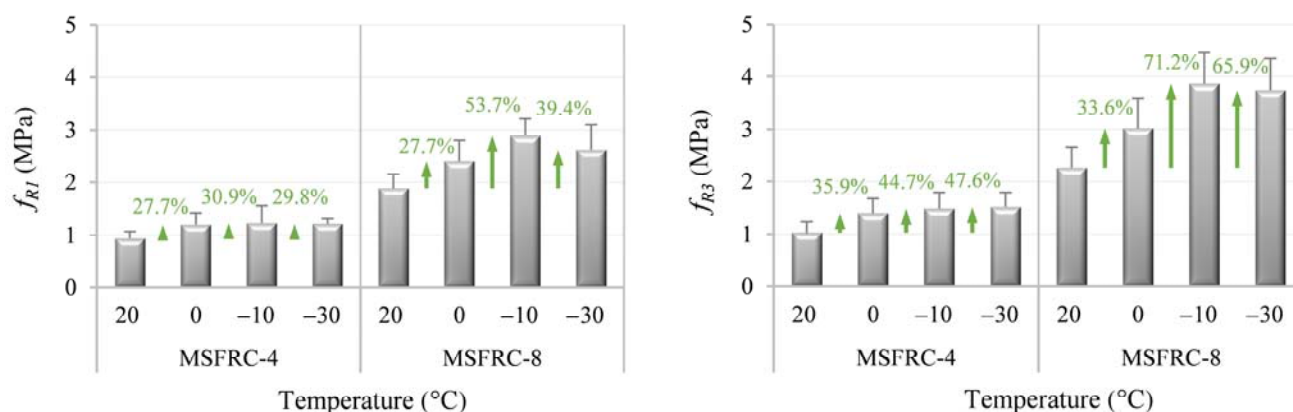


**Figure 5.** Mean values of  $f_{R1}$  and  $f_{R3}$  with corresponding standard deviations of the studied MSFRCs at different temperatures.

Additionally, the effect of the higher fiber content on the enhancement rate of the residual tensile strength (due to temperature reduction) can be stressed: the relatively moderate values of residual tensile strengths in the case of MSFRC-4 did not ensure the continuous increment of post-cracking strength, i.e., both  $f_{R1}$  and  $f_{R3}$  presented similar enhancements of this parameter in the range between 0 °C and −30 °C. Contrarily, MSFRC-8 evidenced a significant increment of residual tensile strengths once temperatures surpassed the threshold temperature magnitude of 0°C—up to 71.2% in comparison with the reference values (at 20 °C). Moreover, the greater increase in  $f_{R3}$  should be highlighted, opposing the enhancement rate due to low temperatures to the increase in  $f_{R1}$ —this phenomenon results from the improvement of the bond capacity in the matrix–fiber interaction that is generally a governing failure mechanism (fiber debonding).

Although the obtained experimental outcome clearly evidenced the increase in pre- and post-cracking flexural strength of the given FRCs, further studies are required to extend the database related to the effect of low temperatures on flexural capacity of the material in question, varying temperature magnitudes, concrete mixes, and fiber type/contents. This will allow to propose a relationship between temperature variation and the flexural strength of FRCs; this relationship, in turn, will allow to characterize the materials at ambient conditions with a subsequent estimation of their potential behavior at more severe conditions.

#### 4. Numerical Analysis

In previous sections, experimental tests have proven the positive effect of low temperatures on FRC by increasing post-cracking strength. Based on the authors' experience, the FRC constitutive equation proposed in the *fib* Model Code 2010 [1], which was set as a reference for design engineers and practitioners to take into account the post-cracking behavior of FRC, needs to be adjusted in order to properly reproduce the latter. The adjustments usually adopted in MSFRC are to reduce residual strength at early stages (for  $\text{CMOD} < 0.5$  mm) since the constitutive equation tends to overestimate the flexural post-

cracking capacity after cracking, whereas the behavior at larger crack openings tends to be underestimated, and the residual strength needs to be increased [65,66]

With that in mind, this section presents a non-linear finite element (FE) simulation to obtain and assess the ratio of residual strength (obtained by means of a numerical simulation) to experimental residual strength ( $f_{R,NL}/f_{R,EXP}$ ) for the FRC mixes (MSFRC-4 and MSFRC-8) tested at different temperatures. In order to derive these  $f_{R,NL}/f_{R,EXP}$  ratios, the strategy adopted is the following: first, non-linear simulations of a beam flexural post-cracking strength test were carried out implementing an FRC-constitutive relationship according to *fib* Model Code 2010 [1]. Figure 6 depicts the schematic representation of the stress-crack width curve for FRC according to the *fib* Model Code 2010 [1]. A full curve is obtained as the combination of the post-cracking response of plain concrete (where  $f_{ctm}$  and  $G_F$  stand for mean tensile concrete strength and fracture energy, respectively) and the fiber contribution through the pull-out mechanism, the first point being  $\sigma_1 = f_{ctm}$  and  $w_1 = 0$  mm, the second point  $\sigma_2$  and  $w_2$  (the intersection between the two curves), and the third one  $\sigma_3 = f_{ctm}$  and  $w_3 = 2.5$  mm. Moreover, since the results did not fit the experimental ones well, the  $f_{R1}$  and  $f_{R3}$  coefficients (to derive constitutive curves according to the *fib* Model Code 2010 constitutive equations) were modified so that the resulting curves fit the values at CMOD of 0.5 and 2.5 mm, which are the crack openings for serviceability and ultimate limit states, respectively. The latter task was undertaken by implementing a back analysis by an iterative trial and error process.

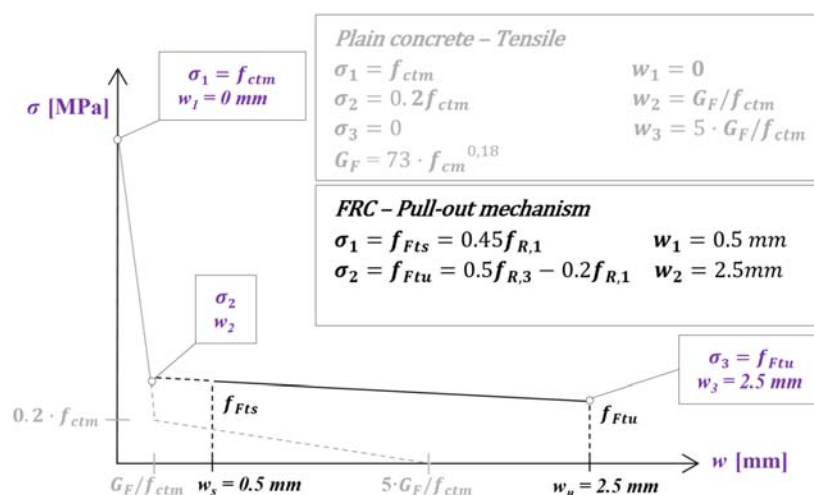


Figure 6. *fib* MC-2010 [1] FRC tensile constitutive equation.

In order to carry out the numerical analysis, non-linear simulations were implemented by means of the commercial finite element (FE) software ABAQUS CAE 2016 [67], as its adequacy in properly reproducing the post-cracking flexural performance of FRC has been successfully proven through an available Concrete Damaged Plasticity (CDP) numerical model [20,66]. CDP is a smeared crack plasticity-based numerical model, which assumes that the main two failure mechanisms are tensile cracking and concrete crushing. Input data are required in terms of uniaxial stress-strain ( $\sigma$ - $\epsilon$ ) curves for both tensile and compressive behavior. In this study, in order to minimize mesh dependence due to different mesh size, the stress-crack width ( $\sigma$ - $w$ ) tensile curve was used instead of  $\sigma$ - $\epsilon$  [67]. The compressive constitutive curve adopted was proposed in the *fib* Model Code 2010 [1], and the CDP magnitude of the parameters adopted for all the simulations were those proposed in ABAQUS Users' Manual [67] for plain concrete, which can be found elsewhere [68].

The adopted 2D model considering plain strain conditions is depicted in Figure 7, which shows the loading and boundary conditions along with the mesh. In agreement

with the experimental test, the boundary conditions were imposed so that vertical displacement was restrained ( $U_y = 0$ ) at both supports and horizontal displacement ( $U_x = 0$ ) in one of them. The loading was applied by means of displacement control using an explicit dynamic algorithm (quasi-static analysis) in order to properly capture the post-cracking performance of FRC. The mesh comprised 485 nodes and 886 triangular linear elements (CPE3) with a mesh size of 20 mm, refined in the mid-section with 5 mm size elements, wherein the mesh size was determined after carrying out a mesh sensitivity analysis.

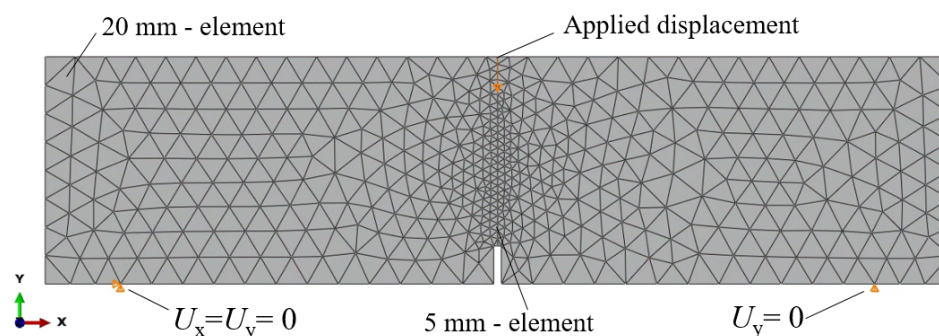


Figure 7. 2D FEM model adopted: mesh and boundary conditions considered.

The results of the non-linear simulations for MSFRC-4 and MSFRC-8 for all temperatures are plotted in Figure 8. The load–CMOD graphs include three curves: experimental results and two from non-linear simulations (1) implementing the *fib* Model Code [1] constitutive equation (FE MC-2010, derived using  $f_{R1}$  and  $f_{R3}$  obtained from the experimental tests presented in Section 3) and (2) using the constitutive curve (FE MC-2010 Modified), adjusted so that the results fit the experimental curve at 0.5 and 2.5 mm. As can be seen, the simulations with FE MC-2010 Modified only fit the experimental data at these points, and hardening is produced in a linear way. Based on the authors' experience, in those cases where the hardening is produced in a curved way, more points would be necessary in the constitutive equation in order to better adjust the experimental outcome [65,66].

It is worth noticing that the ultimate displacement in the *fib* Model Code [1] constitutive curve is 2.5 mm (set as the stress for ultimate limit state analysis). However, in this research study, after 2.5 mm, the constitutive curve smoothly decreases to zero stress, set at  $w = 5$  mm, in order to better capture the flexural bearing capacity of MSFRC at latter stages. Without the last branch of the curve, the maximum post-cracking load of the tests, after the drop due to cracking, cannot be captured since it is produced for crack openings higher than 2.5 mm [65,66].

Table 3 gathers more detailed information regarding  $f_{R1}$  and  $f_{R3}$  parameters for MSFRC-4 and MSFRC-8, respectively. These parameters were used for deriving the constitutive curves obtained from the experimental data and by means of the back analysis. In addition, the table also presents the  $f_{R,NL}/f_{R,EXP}$  ratios for each MSFRC mix and temperature.

Based on the outcome presented in the table, it can clearly be seen that the ranges of the  $f_{R,NL}/f_{R,EXP}$  ratios for either  $f_{R1}$  or  $f_{R3}$  are quite narrow, particularly for  $f_{R1}$ . In this sense, it could be stated that the  $f_{R,NL}/f_{R,EXP}$  ratios are constant despite the increasing post-cracking strength with decreasing temperature. In view of this, in cases where no data are available for low temperatures, and the structure is expected to be subjected to large temperature variations, the same  $f_{R,NL}/f_{R,EXP}$  ratio (for either  $f_{R1}$  and  $f_{R3}$ ) at reference temperature could be taken for the MSFRC design.



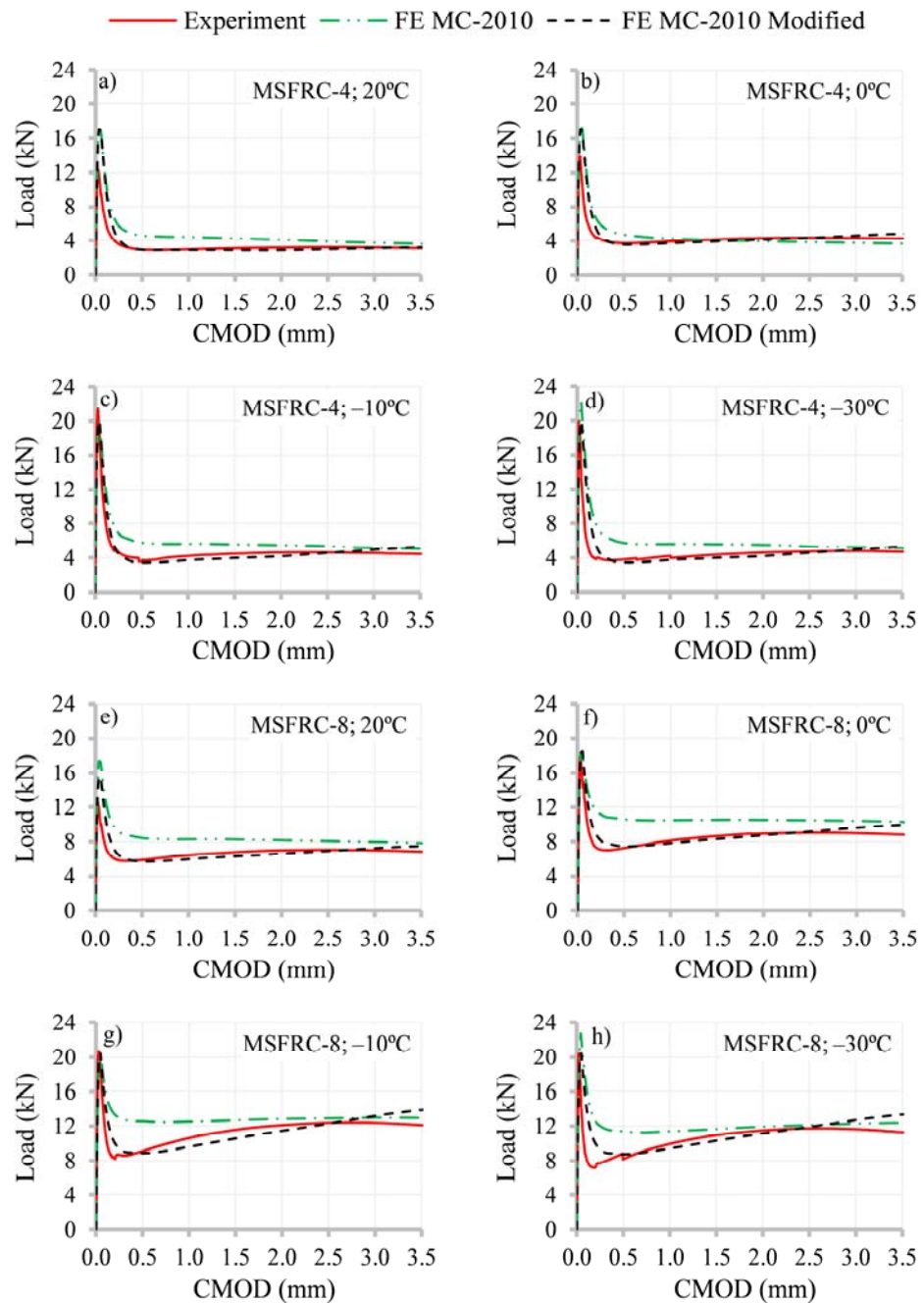
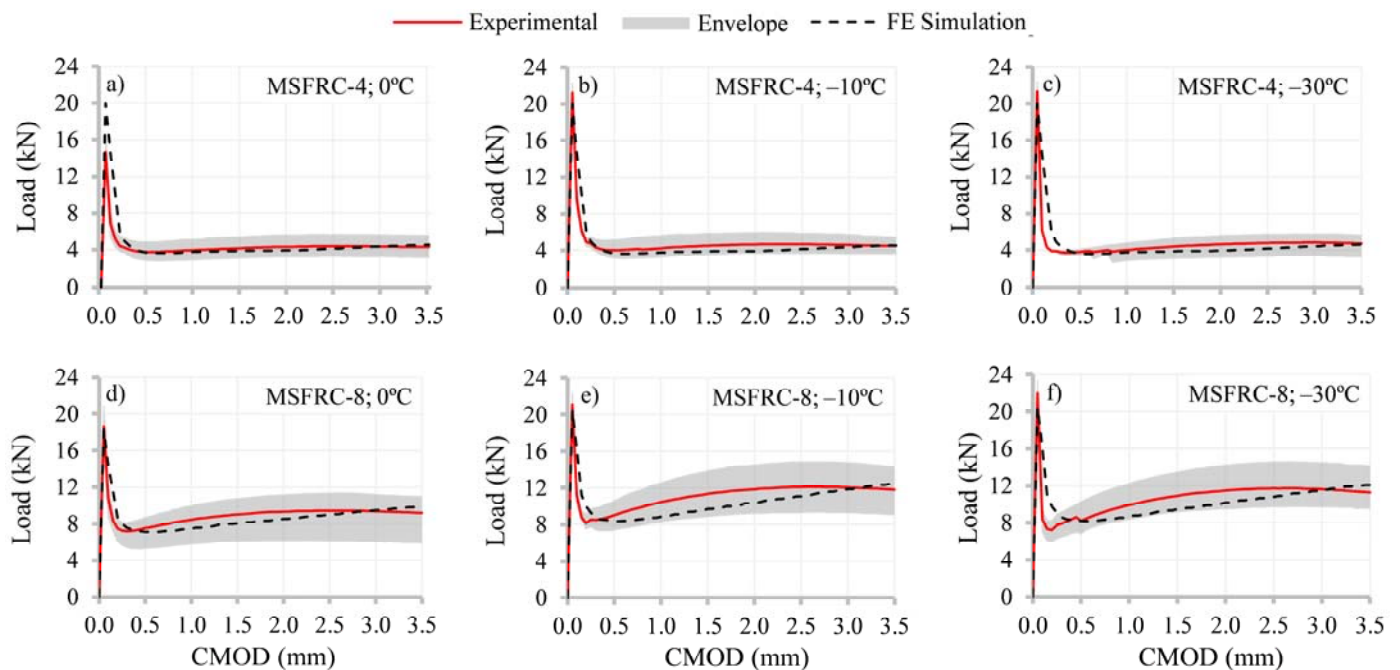


Figure 8. Results for MSFRC-4 and MSFRC-8 at studied temperatures in terms of “load-CMOD”.

Table 3.  $f_{R,NL}/f_{R,EXP}$  ratio for MSFRC-4 and MSFRC-8 at studied temperatures.

	Temperature (°C)	MSFRC-4			MSFRC-8		
		$f_{R,EXP}$ (MPa)	$f_{R,NL}$ (Mpa)	$f_{R,NL}/f_{R,EXP}$	$f_{R,EXP}$ (Mpa)	$f_{R,NL}$ (Mpa)	$f_{R,NL}/f_{R,EXP}$
$f_{R1}$	20	0.94	0.60	0.64	1.88	1.35	0.72
	0	1.20	0.80	0.67	2.4	1.80	0.75
	-10	1.23	0.80	0.65	2.89	2.25	0.78
	-30	1.22	0.80	0.66	2.83	2.25	0.80
$f_{R3}$	20	1.03	1.03	1.00	2.26	2.40	1.06
	0	1.40	1.60	1.14	3.02	3.20	1.06
	-10	1.49	1.80	1.21	3.87	4.60	1.19
	-30	1.52	1.80	1.18	3.75	4.60	1.23

In order to verify this assumption, in Figure 9 were plotted the FE simulations using the residual strengths from the tests at each temperature and multiplied by the  $f_{R,NL}/f_{R,EXP}$  ratio (for either  $f_{R1}$  and  $f_{R3}$ ) at 20 °C (i.e.,  $f_{R1,NL}/f_{R1,EXP} = 0.65$  and  $0.75$  for MSFRC-4 and MSFRC-8, respectively, and  $f_{R3,NL}/f_{R3,EXP} = 1.10$  for both solutions). As can be seen, the differences at CMOD 0.5 and 2.5 mm have a deviation lower than 10% in all cases (Figure 9) which is assumed to be acceptable for engineering design. Moreover, taking into consideration the scatter in the experimental tests of MSFRC post-cracking performance, these new simulations are inside the envelope, which means that this approach is representative of the mechanical performance of each solution of MSFRC.



**Figure 9.** Results in terms of load–CMOD for MSFRC-4 and MSFRC-8 using  $f_{R,NL}/f_{R,EXP}$  at reference temperature to derive the constitutive curves.

It is worth noticing that, in a hypothetical situation in which no tests were performed at low temperatures,  $f_{R1}$  and  $f_{R3}$  at different temperatures could be obtained based on the established relationship “temperature variation–flexural strength” that is to be elaborated once the broader database of the experimental results is developed, as proposed in Section 3.

## 5. Conclusions

In this paper, an experimental program was described following an analysis of low temperature effects on the pre- and post-cracking flexural behavior of macro-synthetic fiber reinforced concrete (MSFRC). In total, 48 prismatic notched beams were tested under a three-point bending configuration, varying temperatures from 20 °C to −30 °C. Moreover, numerical analyses were performed to verify the suitability of the current constitutive models suggested by the *fib* Model Code 2010 for simulating the pre- and post-cracking response of the MSFRCs tested at low temperatures. The following conclusions may be derived from the obtained results:

- Low temperatures led to an increase in the required energy to produce fiber pull-out, and therefore, post-cracking flexural behavior was enhanced:  $f_{R1}$  and  $f_{R3}$  increased to 54% and 71%, respectively, for temperatures below 0°C.
- A greater increase in  $f_{R3}$  at low temperatures (in comparison with the observed values of  $f_{R1}$ ) was observed. This could be due to the confinement effect caused by the shrinkage of the matrix embedding the fibers. This effect seemed to lead to a higher fiber

bond (higher matrix–fiber friction). This outcome is of paramount importance for design procedures at ultimate conditions.

- The numerical analysis adopting the multi-linear constitutive model that is suggested by the *fib* Model Code 2010 evidenced a certain overestimation of the real flexural behavior in cases of studied MSFRC prismatic beams. This phenomenon led to the requirement of introducing correction factors to properly simulate the structural response of the elements in question. Importantly, the imposed correction factors (for both  $f_{R1}$  and  $f_{R3}$ ) were almost identical despite the temperature variation, although the fiber content did have an effect on these values.

The outcome of the described research program reveals the enhanced performance of the given FRCs in terms of pre- and post-cracking flexural strengths—therefore, these phenomena should be taken into account during the design procedures of elements that are to be subjected to low temperatures during transient or in-service conditions. However, further investigation is required to expand the experimental database related to the behavior of FRCs at low temperatures. This will allow to evaluate the “temperature–pre- and post- flexural strength” relationships so that designers and practitioners will only need to carry out the characterization of the required material at ambient conditions (20°C) in order to adequately predict structural behavior at low temperatures.

**Author Contributions:** Conceptualization, A.d.l.F. and N.T.; methodology, S.A. and A.N.; software, A.N.; analysis, S.A., A.N., and I.R.; investigation, I.R.; writing—original draft preparation, S.A. and A.N.; writing—review and editing, A.d.l.F. and N.T.; visualization, S.A.; supervision, A.d.l.F. and N.T.; project administration, A.d.l.F. and N.T.; funding acquisition, A.d.l.F. and N.T. All authors have read and agreed to the published version of the manuscript.

**Funding:** This study has received funding from the European Union’s Horizon 2020 research and innovation program under the Marie Skłodowska-Curie grant agreement no. 836270. The authors also express their gratitude to the Spanish Ministry of Science and Innovation for the financial support received under the scope of the project CREEF (PID2019-108978RB-C32). The first author personally thanks the Department of Enterprise and Education of Catalan Government for providing support through the PhD Industrial Fellowship (2018 DI 77) in collaboration with Smart Engineering Ltd. (UPC’s Spin-Off). The second author, in turn, acknowledges the Spanish Ministry of Science, Innovation and University for providing support through the PhD Industrial Fellowship (DI-17-09390) in collaboration with Smart Engineering Ltd. (UPC’s Spin-Off). Any opinions, findings, conclusions, and/or recommendations in the paper are those of the authors and do not necessarily represent the views of the funding organizations.

**Institutional Review Board Statement:** Not applicable.

**Informed Consent Statement:** Informed consent was obtained from all subjects involved in the study.

**Data Availability Statement:** The data presented in this study are available on request from the corresponding author.

**Conflicts of Interest:** The authors declare no conflict of interest.

## References

1. *Fib. fib Model Code for Concrete Structures 2010*; International Federation for Structural Concrete (FIB): Lausanne, Switzerland, 2013; ISBN 9783433030615.
2. Spanish Ministry of Public Works. Code on Structural Concrete, EHE-08, Permanent Commission of the Concrete; Spanish Ministry of Public Works: Madrid, Spain, 2008.
3. RILEM. Bending Test: Final Recommendations; RILEM TC-162-TDF. *Mater. Struct.* 2002, 35, 579–582.
4. Italian National Research Council CNR. CNR-DT 204/2006 Guide for the Design and Construction of Fiber-Reinforced Concrete Structures; Consiglio Nazionale Delle Ricerche Rome, Italy, 2006.
5. DBV. Guide to Good Practice Steel Fibre Concrete; German Society for Concrete and Construction Technology: Berlin, Germany, 2001.
6. ACI Committee 544. Report on Design and Construction of Steel Fiber-Reinforced Concrete Elevated Slabs; American Concrete Institute: Farmington Hills, MI, USA, 2004. ISBN 9781942727323.
7. Zollo, R.F. Fiber-reinforced Concrete : an Overview after 30 Years of Development. *Cem. Concr. Compos.* 1997, 19, 107–122.

8. Groli, G.; Pérez, A.; Marchetto, F.; Aríñez, F. Serviceability performance of FRC columns under imposed displacements: An experimental study. *Eng. Struct.* **2015**, *101*, 450–464, doi:10.1016/j.engstruct.2015.07.035.
9. Pujadas, P.; Blanco, A.; de la Fuente, A.; Aguado, A. Cracking behavior of FRC slabs with traditional reinforcement. *Mater. Struct. Constr.* **2012**, *45*, 707–725, doi:10.1617/s11527-011-9791-0.
10. Tiberti, G.; Minelli, F.; Plizzari, G.A.; Vecchio, F.J. Influence of concrete strength on crack development in SFRC members. *Cem. Concr. Compos.* **2014**, *45*, 176–185, doi:10.1016/j.cemconcomp.2013.10.004.
11. Conforti, A.; Zerbino, R.; Plizzari, G.A. Influence of steel, glass and polymer fibers on the cracking behavior of reinforced concrete beams under flexure. *Struct. Concr.* **2018**, *20*, 133–143, doi:10.1002/suco.201800079.
12. McMahon, J.A.; Birely, A.C. Service performance of steel fiber reinforced concrete (SFRC) slabs. *Eng. Struct.* **2018**, *168*, 58–68, doi:10.1016/j.engstruct.2018.04.067.
13. Serrano, R.; Cobo, A.; Prieto, M.I.; de las Nieves González, M. Analysis of fire resistance of concrete with polypropylene or steel fibers. *Constr. Build. Mater.* **2016**, *122*, 302–309. <https://doi.org/10.1016/j.conbuildmat.2016.06.055>.
14. Jin, L.; Zhang, R.; Dou, G.; Du, X. Fire resistance of steel fiber reinforced concrete beams after low-velocity impact loading. *Fire Saf. J.* **2018**, *98*, 24–37, doi:10.1016/j.firesaf.2018.04.003.
15. Khaliq, W.; Kodur, V.; Asce, F. Effectiveness of Polypropylene and Steel Fibers in Enhancing Fire Resistance of High-Strength Concrete Columns. *J. Struct. Eng.* **2018**, *144*, 1–12, doi:10.1061/(ASCE)ST.1943-541X.0001981.
16. Carlesso, D.M.; de la Fuente, A.; Cavalaro, S.H.P. Fatigue of cracked high performance fiber reinforced concrete subjected to bending. *Constr. Build. Mater.* **2019**, *220*, 444–455, doi:10.1016/j.conbuildmat.2019.06.038.
17. Germano, F.; Tiberti, G. Post-peak fatigue performance of steel fiber reinforced concrete under flexure. *Mater. Struct.* **2015**, *49*(10), 4229–4245, doi:10.1617/s11527-015-0783-3.
18. Fall, D.; Shu, J.; Rempling, R.; Lundgren, K.; Zandi, K. Two-way slabs: Experimental investigation of load redistributions in steel fibre reinforced concrete. *Eng. Struct.* **2014**, *80*, 61–74.
19. Mahmood, S.M.F.; Foster, S.J.; Valipour, H. Moment redistribution and post-peak behaviour of lightly reinforced-SFRC continuous slabs. *Eng. Struct.* **2021**, *232*, 111834, doi:10.1016/j.engstruct.2020.111834.
20. Nogales, A.; Tošić, N.; de la Fuente, A. Rotation and moment redistribution capacity of fibre reinforced concrete beams: Parametric analysis and code compliance. *Struct. Concr.* **2021** (Online version before inclusion in an issue). <https://doi.org/10.1002/suco.202100350>.
21. Venkateshwaran, A.; Tan, K.H. Moment redistribution in continuous steel-fibre-reinforced concrete slabs. *Struct. Build.* **2020**, *173*, 161–174, doi:<https://doi.org/10.1680/jstbu.17.00152>.
22. Nia, A.A.; Hedayatani, M.; Nili, M.; Sabet, V.A. An experimental and numerical study on how steel and polypropylene fibers affect the impact resistance in fiber-reinforced concrete. *Int. J. Impact Eng.* **2012**, *46*, 62–73, doi:10.1016/j.ijimpeng.2012.01.009.
23. Teng, T.; Chu, Y.-A.; Chang, F.-A.; Shen, B.-C.; Cheng, D.-S. Development and validation of numerical model of steel fiber reinforced concrete for high-velocity impact. *Comput. Mater. Sci.* **2008**, *42*, 90–99, doi:10.1016/j.commatsci.2007.06.013.
24. Rai, B.; Singh, N.K. Statistical and experimental study to evaluate the variability and reliability of impact strength of steel-polypropylene hybrid fiber reinforced concrete. *J. Build. Eng.* **2021**, *44*, 102937, doi:10.1016/j.jobbe.2021.102937.
25. Vivas, J.C.; Zerbino, R.; Torrijos, M.; Giaccio, G. A test procedure for evaluating the impact behaviour of fibre reinforced concrete. *Mater. Struct.* **2021**, *54*, 208, doi:10.1617/s11527-021-01804-9.
26. Liu, X.; Sun, Q.; Yuan, Y.; Taerwe, L. Comparison of the structural behavior of reinforced concrete tunnel segments with steel fiber and synthetic fiber addition. *Tunn. Undergr. Space Technol.* **2020**, *103*, 103506. <https://doi.org/10.1016/j.tust.2020.103506>.
27. Conforti, A.; Trabucchi, I.; Tiberti, G.; Plizzari, G.A.; Caratelli, A.; Meda, A. Precast tunnel segments for metro tunnel lining: A hybrid reinforcement solution using macro-synthetic fibers. *Eng. Struct.* **2019**, *199*, 109628, doi:10.1016/j.engstruct.2019.109628.
28. de la Fuente, A.; Pujadas, P.; Blanco, A.; Aguado, A. Experiences in Barcelona with the use of fibres in segmental linings. *Tunn. Undergr. Sp. Technol.* **2012**, *27*, 60–71, doi:10.1016/j.tust.2011.07.001.
29. Aidarov, S.; Mena, F.; de la Fuente, A. Structural response of a fibre reinforced concrete pile-supported flat slab: Full-scale test. *Eng. Struct.* **2021**, *239*, 112292. <https://doi.org/10.1016/J.ENGSTRUCT.2021.112292>.
30. Leporace-Guimil, B.; Mudadu, A.; Conforti, A.; Plizzari, G.A. Influence of fiber orientation and structural-integrity reinforcement on the flexural behavior of elevated slabs. *Eng. Struct.* **2021**, 113583. <https://doi.org/10.1016/j.engstruct.2021.113583>.
31. di Prisco, M.; Colombo, M.; Pourzarabi, A. Biaxial bending of SFRC slabs: Is conventional reinforcement necessary? *Mater. Struct. Constr.* **2019**, *52*, 1–15, doi:10.1617/s11527-018-1302-0.
32. de la Fuente, A.; Aguado, A.; Molins, C.; Armengou, J. Innovations on components and testing for precast panels to be used in reinforced earth retaining walls. *Constr. Build. Mater.* **2011**, *25*, 2198–2205, doi:10.1016/j.conbuildmat.2010.11.003.
33. Meda, A.; Plizzari, G.A.; Riva, P. Fracture behavior of SFRC slabs on grade. *Mater. Struct. Constr.* **2004**, *37*, 405–411, doi:10.1617/14093.
34. Meda, A.; Plizzari, G.A. New design approach for steel fiber-reinforced concrete slabs-on-ground based on fracture mechanics. *ACI Struct. J.* **2004**, *101*, 298–303, doi:10.14359/13089.
35. Aidarov, S.; Mena, F.; de la Fuente, A. Self-compacting Steel Fibre Reinforced Concrete: Material Characterization and Real Scale Test up to Failure of a Pile Supported Flat Slab. In Proceedings of the RILEM-fib International Symposium on Fibre Reinforced Concrete, Valencia, Spain, 20–22 September 2021; Springer, Cham, Switzerland, 2021; pp. 702–713.



36. Alberti, M.G.; Enfedaque, A.; Gálvez, J.C. The effect of fibres in the rheology of self-compacting concrete. *Constr. Build. Mater.* **2019**, *219*, 144–153, doi:10.1016/j.conbuildmat.2019.05.173.
37. Cavalaro, S.H.P.; Aguado, A. Intrinsic scatter of FRC: an alternative philosophy to estimate characteristic values. *Mater. Struct. Constr.* **2015**, *48*, 3537–3555, doi:10.1617/s11527-014-0420-6.
38. Tiberti, G.; Germano, F.; Mudadu, A.; Plizzari, G.A. An overview of the flexural post-cracking behavior of steel fiber reinforced concrete. *Struct. Concr.* **2018**, *19*(3), 695–718. <https://doi.org/10.1002/suco.201700068>.
39. Parmentier, B., De Grove, E., Vandewalle, L. and Van Rickstal, F., 2008. Dispersion of the mechanical properties of FRC investigated by different bending tests. Tailor made concrete structures, pp.507-512.
40. Amin, A.; Gilbert, R.I. Instantaneous crack width calculation for steel fiber-reinforced concrete flexural members. *ACI Struct. J.* **2018**, *115*, 535–543, doi:10.14359/51701116.
41. Colombo, M.; Martinelli, P.; di Prisco, M. On the evaluation of the structural redistribution factor in FRC design: a yield line approach. *Mater. Struct.* **2017**, *50*, 1–18, doi:10.1617/s11527-016-0969-3.
42. de la Fuente, A.; Escariz, R.C.; de Figueiredo, A.D.; Aguado, A. Design of macro-synthetic fibre reinforced concrete pipes. *Constr. Build. Mater.* **2013**, *43*, 523–532, doi:10.1016/j.conbuildmat.2013.02.036.
43. di Prisco, M.; Martinelli, P.; Parmentier, B. On the reliability of the design approach for FRC structures according to fib Model Code 2010: the case of elevated slabs. *Struct. Concr.* **2016**, *17*, 588–602, doi:10.1002/suco.201500151.
44. di Prisco, M.; Plizzari, G.; Vandewalle, L. Fibre reinforced concrete: New design perspectives. *Mater. Struct. Constr.* **2009**, *42*, 1261–1281, doi:10.1617/s11527-009-9529-4.
45. Facconi, L.; Minelli, F. Verification of structural elements made of FRC only: A critical discussion and proposal of a novel analytical method. *Eng. Struct.* **2017**, *131*, 530–541, doi:10.1016/j.engstruct.2016.10.034.
46. Facconi, L.; Plizzari, G.; Minelli, F. Elevated slabs made of hybrid reinforced concrete: Proposal of a new design approach in flexure. *Struct. Concr.* **2019**, *20*, 52–67, doi:10.1002/suco.201700278.
47. Enfedaque, A.; Alberti, M.G.; Gálvez, J.C.; Domingo, J. Numerical simulation of the fracture behaviour of glass fibre reinforced cement. *Constr. Build. Mater.* **2017**, *136*, 108–117, doi:10.1016/j.conbuildmat.2016.12.130.
48. Enfedaque, A.; Alberti, M.G.; Galvez, J. Analysis of the Versatility of Multi-Linear Softening Functions Applied in the Simulation of Fracture Behaviour of Fibre-Reinforced Cementitious Materials. *Materials* **2019**, *12*, 3656. <https://doi.org/10.3390/ma12223656>.
49. Enfedaque, A.; Alberti, M.G.; Galvez, J.; Cabanas, P. Numerical Simulation of the Fracture Behavior of High-Performance Fiber-Reinforced Concrete by Using a Cohesive Crack-Based Inverse Analysis. *Materials* **2022**, *15*, 71. <https://doi.org/10.3390/ma15010071>.
50. de Maio, U.; Fantuzzi, N.; Greco, F.; Leonetti, L.; Pranno, A. Failure Analysis of Ultra High-Performance Fiber-Reinforced Concrete Structures Enhanced with Nanomaterials by Using a Diffuse Cohesive Interface Approach. *Nanomaterials* **2020**, *10*, 1792. <https://doi.org/10.3390/nano10091792>.
51. di Prisco, M.; Martinelli, P.; Dozio, D. The structural redistribution coefficient  $K_{rd}$ : A numerical approach to its evaluation. *Struct. Concr.* **2016**, *17*, 390–407. <https://doi.org/10.1002/suco.201500118>.
52. Фотограф Сергей Филинин Available online: <https://sergeyfilinin.ru/#portfolio> (accessed on Dec 25, 2021).
53. Lee, G.C.; Shih, S.; Chang, K.C. Mechanical Properties of Concrete at Low Temperature. *J. Cold Reg. Eng.* **1988**, *2*, 13–24.
54. Xie, J.; Yan, J.B. Experimental studies and analysis on compressive strength of normal-weight concrete at low temperatures. *Struct. Concr.* **2018**, *19*, 1235–1244, doi:10.1002/suco.201700009.
55. Montejo, L.A.; Sloan, J.E.; Kowalsky, M.J.; Hassan, T. Cyclic Response of Reinforced Concrete Members at Low Temperatures. *J. Cold Reg. Eng.* **2008**, *22*, 79–102, doi:10.1061/(asce)0887-381x(2008)22:3(79).
56. Pigeon, M.; Cantin, R. Flexural properties of steel fiber-reinforced concretes at low temperatures. *Cem. Concr. Compos.* **1998**, *20*, 365–375, doi:10.1016/S0958-9465(98)00017-1.
57. Caballero-Jorna, M.; Roig-Flores, M.; Serna, P. Short-term effects of moderate temperatures on the mechanical properties of steel and macrosynthetic fiber reinforced concretes. In Proceedings of the RILEM-Fib X International Symposium on Fibre Reinforced Concrete BEFIB 2021, Valencia, Spain, 20–22 September 2021; Springer: Berlin/Heidelberg, Germany, 2021.
58. Richardson, A.; Ovington, R. Temperature related steel and synthetic fibre concrete performance. *Constr. Build. Mater.* **2017**, *153*, 616–621, doi:10.1016/j.conbuildmat.2017.07.101.
59. CEN. EN 14651. Test Method for Metallic Fibre Concrete. Measuring the Flexural Tensile Strength (Limit of Proportionality (LOP), Residual); European Committee for Standardization: Bruxelles, Belgium, 2007. ISBN 9780580610523.
60. CEN. EN 12350-2:2019. Testing Fresh Concrete. Slump Test; European Committee for Standardization: Bruxelles, Belgium, 2019.
61. König, G.; Kützing, L. Modelling the increase of ductility of HPC under compressive forces—A fracture mechanical approach. In Proceedings of the Third International RILEM Workshop on High Performance Fiber Reinforced Cement Composites, Mainz, Germany, 16–19 May 1999; RILEM Publications SARL: Bagneux, France, 1999; pp. 251–260.
62. Mena, F.; Aidarov, S.; de la Fuente, A. Hormigones autocompactantes reforzados con fibras para aplicaciones con alta responsabilidad estructural. Campaña experimental en laboratorio. In Proceedings of the III Congreso de Consultores de Estructuras; Barcelona, Spain, 3–5 April 2019; pp. 1–10.
63. Bentur, A.; Mindess, S. *Fibre Reinforced Cementitious Composites*; Taylor & Francis: Abingdon, UK, 2007.
64. Kim, J.K.; Mai, Y.-W. High strength, high fracture toughness fibre composites with interface control-A review. *Compos. Sci. Technol.* **1991**, *41*, 333–378, doi:10.1016/0266-3538(91)90072-W.

65. Galeote, E.; Nogales, A.; de la Fuente, A. Analysis of design constitutive model for plastic fibre reinforced concrete through inverse analysis. In Proceedings of the 75th RILEM Week, Merida, Mexico, 29 August–3 September 2021; Springer: Berlin/Heidelberg, Germany, 2021.
66. Nogales, A.; Galeote, E.; de la Fuente, A. Finite element analysis characterization of macro synthetic fibre reinforced concrete constitutive equation. In Proceedings of the 75th RILEM Week, Merida, Mexico, 29 August–3 September 2021; Springer: Berlin/Heidelberg, Germany, 2021.
67. Dassault Systèmes Simulia *Abaqus CAE User's Manual (6.12)*; Dassault Systèmes, Providence, 2012;
68. Nogales, A.; de la Fuente, A. Elevated Flat Slab of Fibre Reinforced Concrete Non-Linear Simulation Up to Failure; Springer International Publishing: Berlin/Heidelberg, Germany, 2022; Volume 36. ISBN 9783030837198.